PCCP

Comparative trajectory surface hopping study for the $Li + Li_2(X\,^1\Sigma_g^+)$, $Na + Li_2(X\,^1\Sigma_g^+)$ and $Li + Na_2(X\,^1\Sigma_g^+)$ dissociation reactions

J. M. C. Marques, A. I. Voronin and A. J. C. Varandas*

Departamento de Química, Universidade de Coimbra, P-3049 Coimbra Codex, Portugal

Received 2nd March 1999, Accepted 12th April 1999

Trajectory surface hopping calculations are presented for the $Li + Li_2$ ($X\,^1\Sigma_g^+$), $Na + Li_2$ ($X\,^1\Sigma_g^+$) and $Li + Na_2$ ($X\,^1\Sigma_g^+$) dissociation reactions using realistic potential energy surfaces for the lowest doublet states of Li_3, $NaLi_2$, and $LiNa_2$. The calculations were carried out over the range of translational energies E_{tr} = 11.5–80.0 kcal mol^{-1} and vibrational quantum numbers $v = 0$, 10, and 20 for Li_2 ($X\,^1\Sigma_g^+$) and Na_2 ($X\,^1\Sigma_g^+$). A comparison with previous results for $Li + Li_2$ ($X\,^1\Sigma_g^+$) (*J. Phys. Chem. A*, 1998, **102**, 6057) is presented. The behavior of the calculated dissociative cross sections as a function of translational energy shows the importance of nonadiabatic effects for the whole range of energies in the three systems.

1 Introduction

Following previous work,[1] we continue our investigation of nonadiabatic effects for the collision-induced dissociation of alkali metal triatomics. In that study,[1] we have reported an investigation by a semiclassical surface hopping method[2–4] of adiabatic and nonadiabatic $Li + Li_2$ ($X\,^1\Sigma_g^+$, v, $j = 10$) → Li + Li + Li dissociative channels and the effect of the D_{3h} conical intersection on dissociative cross sections for the processes occurring *via* the ground and excited sheets of the two-valued Li_3 potential energy surface.[2,3] Moreover, we have investigated the influence of vibrational excitation on the dissociative process and showed that dissociative cross sections are enhanced as v increases from $v = 0$ to 20. It was also shown that nonadiabatic effects play a significant role in the dynamics of collision-induced dissociation for the $Li + Li_2$ ($X\,^1\Sigma_g^+$, v, $j = 10$) system. For the dynamics studies we have used a realistic two-valued semiempirical potential energy surface[3] which has been obtained by using the double many-body expansion method[4,5] and taking into account the normalization of the kinetic field.[6]

In this work, we focus on the collision-induced dissociation of Li_2 ($X\,^1\Sigma_g^+$, v, j) by a Na atom, and Na_2 ($X\,^1\Sigma_g^+$, v, j) by a Li atom. The exchange reactions of alkali metal atoms and alkali metal diatomic molecules $M' + M_2$ (v, j) (M and M′ are alkali metal atoms) have been the subject of many studies from both the experimental and theoretical points of view (see refs. 7 and 8, and references therein). The motivation for such interest stems from the fact that these reactions are expected to occur on barrierless potential energy surfaces, and hence are important prototypes of reactions controlled by long-range forces. They are also convenient for experimental studies because the diatomics Li_2, Na_2, and the hybrid LiNa can be prepared and detected by using optical pumping with tunable lasers. However, the dissociation processes have received much less attention. We choose for our investigation the $NaLi_2$ and $LiNa_2$ systems because semi-empirical valence bond potential energy surfaces which rest on a generalized-London–Eyring–Polanyi–Sato (generalized-LEPS) formulation are available. Since the potential energy surfaces for the Li_3, $NaLi_2$ and $LiNa_2$ systems have different topographical features and a different mass combination (LLL, HLL and LHH, respectively) we have performed dynamics studies of collision-induced dissociation for $Na + Li_2$ and $Li + Na_2$ and compared the results among each other as well as with those obtained from our previous investigation.[1]

Details of the paper are as follows: Section 2 summarizes the main topographical features of the potential energy surfaces for $NaLi_2$, $LiNa_2$, and Li_3 systems and reviews the computational procedures. The main trajectory results for the three systems are reported in Section 3. Section 4 compares the results for the title systems and presents a detailed discussion. The conclusions are in Section 5.

2 Potential energy surfaces and methodology

An important requirement for the accurate description of the nonadiabatic dynamics of collision-induced dissociation of the alkali metal trimers is to have an accurate analytical representation of the relevant two-valued potential energy surfaces. In the present study we have used realistic two-valued potential energy surfaces for Li_3,[2,3] $NaLi_2$,[9] and $LiNa_2$.[9] The latter two are based on a generalized-LEPS formalism and correctly reproduce the experimental dissociation energy while the former, henceforward called DMBE III, was obtained from the double many-body expansion[4,5] (DMBE) method including normalization of the kinetic field.[6] In all cases, the diatomic fragments are accurate from the valence region up to the van der Waals region,[9–11], which has been accomplished by means of a universally effective potential for the triplet curve of the diatomic fragments.

Fig. 1 shows an isoenergetic contour plot for both the upper [panel (a)] and lower [panel (b)] sheets of the Li_3 potential energy surface. Clearly visible from panel (b) of this figure are the three equivalent minima and the D_{3h} conical intersection, while panel (a) shows the corresponding repulsive upper sheet with its value of lowest energy placed at the intersection locus. In Fig. 2, we present a similar isoenergetic contour plot for $NaLi_2$. As follows from this plot, the optimal structure has C_{2v} symmetry and corresponds to a very flat region of the potential energy surface. Also visible from Fig. 2 is the peak where the upper and lower sheets of the potential energy

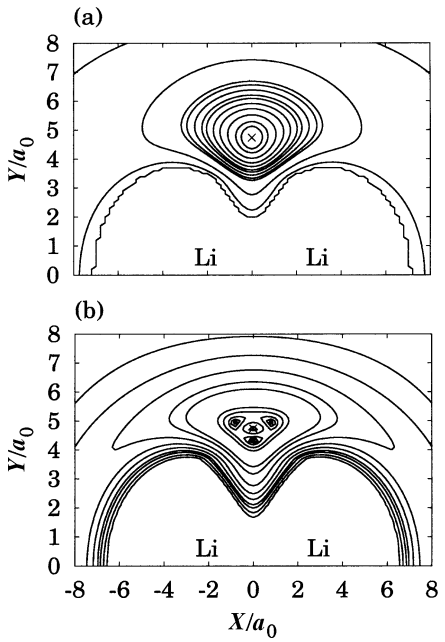

Fig. 1 Isoenergetic contour plot for a Li atom moving around a partially relaxed $Li_2(X\,^1\Sigma_g^+)$ [or Li_2 $(b\,^3\Sigma_u^+)$] diatomic ($4.5 \leqslant R_{Li-Li}/a_0 \leqslant 8.5$), which lies along the x axis with the center of mass fixed at the origin: (a) upper sheet; (b) lower sheet. Minimum energy structures in the lower sheet and conical intersection are in both panels indicated by ● and ×, respectively.

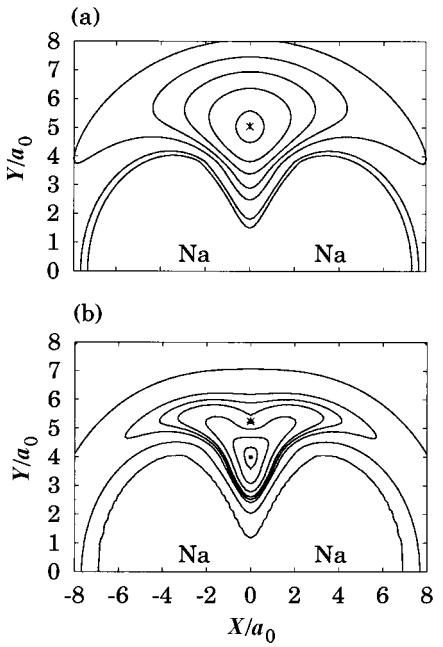

Fig. 3 Isoenergetic contour plot for a Li atom moving around a partially relaxed $Na_2(X\,^1\Sigma_g^+)$ [or $Na_2(b\,^3\Sigma_u^+)$] diatomic ($4.5 \leqslant R_{Na-Na}/a_0 \leqslant 8.5$), which lies along the x axis with the center of mass fixed at the origin: (a) upper sheet; (b) lower sheet. Symbols are as in Fig. 1.

surface join at the Jahn–Teller conical intersection. For the homonuclear trimers (Li_3) this peak becomes central and corresponds to an equiliateral triangular geometry surrounded by a trough containing three equilateral potential wells, while for the $NaLi_2$ it corresponds to a C_{2v} structure surrounded by a trough containing oscillators with twofold symmetry.

Fig. 3 shows the corresponding isoenergetic contour plots for the upper [panel (a)] and lower [panel (b)] sheets of the $LiNa_2$ potential energy surface. The notable features for the present dynamics study are the C_{2v} minimum and the conical intersection, both visible in panel (b) of Fig. 3. In contrast, the repulsive character of the upper sheet is shown in panel (a). Note from panel (b) of Fig. 3 that the perpendicular attack of the Li atom to Na_2 leads, at first, to the conical intersection structure, while for the two other systems (Fig. 1 and 2) the incoming atom is first attracted by potential minima.

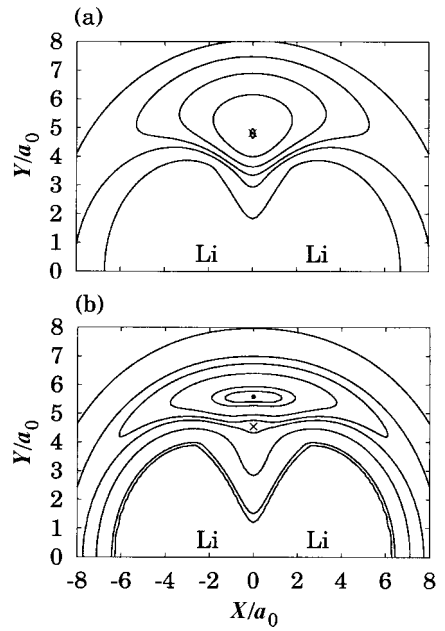

Fig. 2 Isoenergetic contour plot for a Na atom moving around a partially relaxed $Li_2(X\,^1\Sigma_g^+)$ [or $Li_2(b\,^3\Sigma_u^+)$] diatomic ($4.5 \leqslant R_{Li-Li}/a_0 \leqslant 8.5$), which lies along the x axis with the center of mass fixed at the origin: (a) upper sheet; (b) lower sheet. Symbols are as in Fig. 1.

In the schematic diagram of Fig. 4 we compare the main energetic features of Li_3 DMBE III potential energy surface and the generalized-LEPS potentials for $Na + Li_2$ and $Li + Na_2$. As seen from this figure, the dissociative channels are 24.4 kcal mol^{-1}, 24.2 kcal mol^{-1}, and 16.8 kcal mol^{-1} above the motionless reactants $Li + Li_2(X\,^1\Sigma_g^+)$, $Na + Li_2(X\,^1\Sigma_g^+)$, and $Li + Na_2(X\,^1\Sigma_g^+)$, respectively. Although both $Li + Li_2$ and $Na + Li_2$ contain a Li_2 diatomic, we should note that the built-in diatomic potentials are slighly different and hence the dissociation energies, as well as the vibrational–rotational levels, show small discrepancies. It is also seen from Fig. 4 that the internal states ($v = 0$, $j = 10$), ($v = 10$, $j = 10$), and ($v = 20$, $j = 10$) are closer for Na_2 than for Li_2 due to mass effects. Moreover, all channels are above the energy of the reactants (which we have taken as zero) for $Li + Li_2$ and $Na + Li_2$ while, for $Li + Na_2$, the formation of $LiNa(^1\Sigma^+)$ falls 3.3 kcal mol^{-1} below the energy of the reactants. Note that, for $NaLi_2$ ($LiNa_2$), the conical intersection arises for C_{2v} geometries and is 3.2 kcal mol^{-1} (or 2.9 kcal mol^{-1}) above the C_{2v} ($^2A_1$ or $^2B_2$) minimum.

We now turn to describe the trajectory surface hopping (TSH) methodology used in the present dynamics study. For this we have used our own trajectory surface hopping computer code which was described elsewhere.[1] The approach shows a close similarity with the TSH method proposed by Tully and Preston.[12] Thus, at the beginning, each trajectory is started in the ground adiabatic potential energy surface $V_1(\boldsymbol{R})$, where $\boldsymbol{R} = (R_1, R_2, R_3)$ denotes the full set of internuclear coordinates. The difference $\Delta V_{12} = V_1 - V_2$ between two sheets of the potential energy surface is then examined after each integration step. Whenever ΔV_{12} reaches a minimum we use the three last points of V_1 and V_2 to obtain the parameters in the Landau–Zener formula for the probability of non-adiabatic transition. As usual, a random number is generated to choose the sheet of the potential energy surface in which

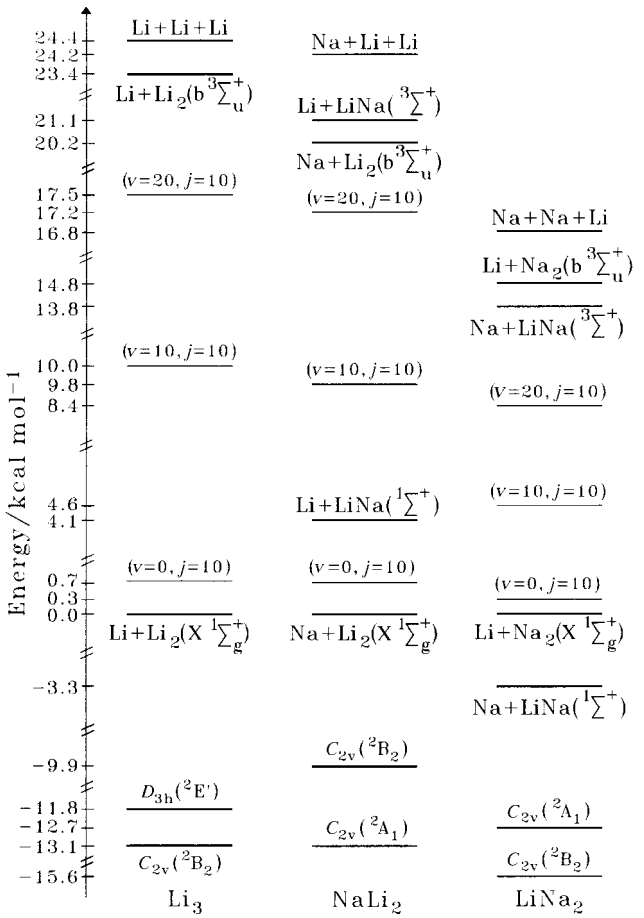

Fig. 4 Schematic diagram of the main energetic features for the title systems. The zero of energy corresponds in the three cases to the motionless reactants.

the trajectory is going to be continued. After a hop to the other potential energy surface, the momenta on the new potential surface are adjusted according to the procedure suggested by Tully and Preston.[12] This adjustment warrants conservation of both the energy and momenta along the trajectory. It should be noted that there are currently more sophisticated semiclassical methods for the study of nonadiabatic dynamics. In particular, there are schemes based on the trajectory propagation with simultaneous integration of the coupled semiclassical equations for the coefficients of the electronic wave function.[13,14] However, such methods have difficulties in practical application. The major problem is perhaps the requirement of an accurate determination of the nonadiabatic coupling elements along the trajectory, in particular, if we have a knowledge only of the semiempirical adiabatic potential energy surfaces. Thus, it is difficult to choose amongst the available TSH variants, because all lead often only to qualitative agreement with quantum calculations.[15,16] An additional reason for our choice is the fact that in our previous study we have used the TSH method with the Landau–Zener probability and our goal in the present work is to compare the results for different alkali metal systems based on the available potential energy surfaces.

3 Trajectory surface hopping calculations

We have used the TSH method described in Section 2 to run a total of 5000 trajectories for each set of initial conditions. The title systems have been studied in the range of translational energies $11.5 \leqslant E_{tr}/\text{kcal mol}^{-1} \leqslant 80$; as before,[1] the initial diatomics have been prepared in the ($v = 0$, $j = 10$) internal state. To get additional information about the influence of the conical intersection seam on the dynamics of the title systems we have also computed trajectories using only the corresponding lowest adiabatic potential energy surfaces. These calculations have been performed at $E_{tr} = 11.5$, 25, 30, 40, 50, and 80 kcal mol^{-1} for Na + Li_2, and at $E_{tr} = 17.5$, 25, 50, and 80 kcal mol^{-1} for Li + Na_2; for Li + Li_2, in addition to using the results reported elsewhere,[1] we have calculated an extra point for $E_{tr} = 80$ kcal mol^{-1}. Moreover, we have run batches of 5000 trajectories for $E_{tr} = 25.0$ kcal mol^{-1} and $v = 10$, 20 to study the dependence dissociation cross section on the initial vibrational excitation.

Since the total energy of the collisional particles is always above the dissociation limit, we may have five different outcomes: non-reactive, reactive and dissociative trajectories both in lower and upper sheets. Although giving special emphasis to dissociative events, both adiabatic (N^{a}_{dis}) and nonadiabatic (N^{na}_{dis}), we present in Table 1 and Table 2 the number of reactive trajectories on the lower adiabatic sheet (N^{a}_{r}), and all the reactive channels other than total dissociation on the upper sheet (N^{na}_{r}). It is assumed that the number of events leading to quasibond states is negligible.

The optimum integration time-step was found to be ~2.0 au for all sets of initial conditions, which warrants conservation of total energy and momentum with an error less than 10^{-6} au for most trajectories, while the maximum value of the impact parameter b_{max} has been optimized by taking into account only the dissociative process. The optimum values of b_{max} are given in Tables 1 and 2 for all calculations on Na + Li_2 and Li + Na_2, respectively; for Li + Li_2, the value of b_{max} for the calculation at $E_{tr} = 80$ kcal mol^{-1} using only the lowest sheet of DMBE III potential energy surface is 5.7 a_0, while the values for the remaining studies have been given elsewhere.[1] In turn, Fig. 5 and Fig. 6 show the opacity functions for dissociation in the three title systems, *i.e.*, $P_d(b)$ *vs.* reduced impact parameter, at $E_{tr} = 25$ kcal mol^{-1} with ($v = 0$, $j = 10$), ($v = 10$, $j = 10$), and ($v = 20$, $j = 10$), while Fig. 7 presents the corresponding values at $E_{tr} = 80$ kcal mol^{-1} and ($v = 0$, $j = 10$). Note from these figures that the opacity functions for the TSH adiabatic dissociation resemble the behavior of those obtained in the calculations using only the lowest

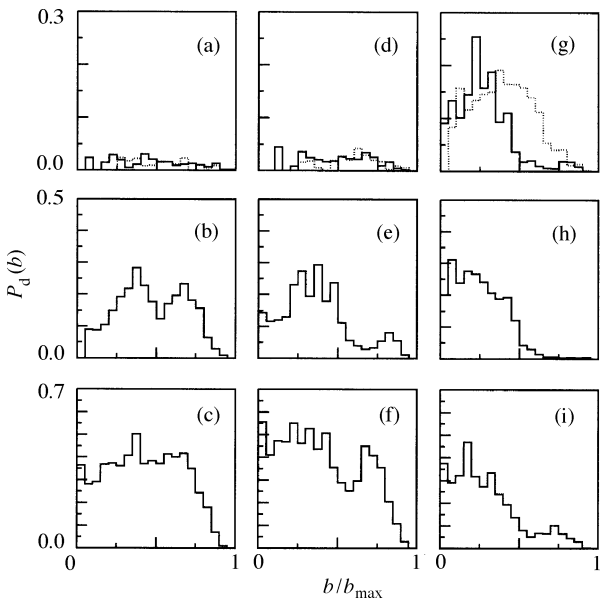

Fig. 5 Opacity function for the adiabatic dissociative process arising from the TSH calculations (———) or using only the lowest sheet of the potential energy surface (·····): (a)–(c) Li + Li_2; (d)–(f) Na + Li_2; (g)–(i) Li + Na_2. The initial translational energy was fixed at $E_{tr} = 25$ kcal mol^{-1}, while the vibrational quantum number has taken the values $v = 0$ [(a), (d), and (g)], $v = 10$ [(b), (e), and (h)], and $v = 20$ [(c), (f), and (i)].

Table 1 Summary of the trajectory calculations for the Na + $Li_2(\tilde{X}\,^1\Sigma_g^+)$ reactions[a]

			Lower sheet			Upper sheet			
E_{tr}/kcal mol^{-1}	v	b_{max}/a_0	N_{dis}^a	N_r^a	σ_d^a/a_0^2	N_{dis}^{na}	N_r^{na}	σ_d^{na}/a_0^2	σ_{tot}/a_0^2[b]
11.5	0	8.00	0	1564[c]	—	0	0	—	—
		8.40	0	1382[d]	—	—	—	—	—
25.0	0	6.20	80	1874	1.9 ± 0.2	76	353	1.8 ± 0.2	3.8 ± 0.3
		6.20	69	2117	1.7 ± 0.2	—	—	—	—
	10	12.00	439	775	39.7 ± 1.8	102	58	9.2 ± 0.9	48.9 ± 2.0
	20	14.50	1404	365	185.5 ± 3.8	105	24	13.9 ± 1.3	199.3 ± 4.3
27.0	0	6.25	168	1686	4.1 ± 0.3	159	315	3.9 ± 0.3	8.0 ± 0.4
28.5	0	6.40	231	1570	5.9 ± 0.4	231	291	5.9 ± 0.4	11.9 ± 0.5
30.0	0	6.45	273	1448	7.1 ± 0.4	251	259	6.6 ± 0.4	13.7 ± 0.6
		6.50	297	1722	7.9 ± 0.4	—	—	—	—
32.5	0	6.50	404	1251	10.7 ± 0.5	229	242	6.1 ± 0.4	16.8 ± 0.6
35.0	0	6.45	532	1282	13.9 ± 0.6	267	232	7.0 ± 0.4	20.9 ± 0.7
40.0	0	6.30	816	1033	20.4 ± 0.7	308	251	7.7 ± 0.4	28.0 ± 0.7
		6.60	787	1160	21.5 ± 0.7	—	—	—	—
45.0	0	6.20	977	951	23.6 ± 0.7	328	199	7.9 ± 0.4	31.5 ± 0.8
50.0	0	6.20	1121	695	27.1 ± 0.7	372	231	9.0 ± 0.4	36.1 ± 0.8
		6.40	1260	818	32.4 ± 0.8	—	—	—	—
80.0	0	6.20	1657	234	40.0 ± 0.8	401	155	9.7 ± 0.5	49.7 ± 0.8
		6.40	1780	277	45.8 ± 0.9	—	—	—	—

[a] For E_{tr} = 11.5, 25, 30, 40, 50 and 80 kcal mol^{-1} (all $v = 0$), the second entry refers to the trajectory calculation where only the lower-sheet of the potential energy surface was considered. [b] Note that $\sigma_{tot} = \sigma_d^a + \sigma_d^{na}$. [c] The corresponding reactive cross section is $\sigma_r^a = 62.9 \pm 1.3\ a_0^2$. [d] The corresponding reactive cross section is $\sigma_r^a = 61.3 \pm 1.4\ a_0^2$.

sheet of the corresponding two-valued potential energy surfaces, especially for Li + Li_2 and Na + Li_2.

Once we have b_{max} and the number of adiabatic and nonadiabatic dissociative trajectories for each set of initial conditions, it is possible to calculate the corresponding cross sections according to the expression

$$\sigma_d^x = \pi b_{max}^2 N_{dis}^x/N \quad (1)$$

where $N = 5000$ trajectories and x denotes the superscripts a (adiabatic) or na (nonadiabatic). The corresponding 68% standard errors are given by

$$\Delta\sigma_d^x = \sigma_d^x[(N - N_{dis}^x)/NN_{dis}^x]^{1/2} \quad (2)$$

3.1 Li + Li_2: an overview

Since the main results for the Li + Li_2 dissociation reaction have been presented in ref. 1, we recall here only the most important features, with the reader being referred to the original work for details. In turn, we show in Fig. 8(a) the dissociative cross sections (adiabatic, nonadiabatic, and total) as a function of the initial translational energy, which have been obtained using the TSH method previously described. The notable feature from this figure is the fact that the Li + Li_2 dissociative cross section tends to increase with increasing translational energy, while the nonadiabatic values remain approximately constant for translational energies above 30 kcal mol^{-1} or so. Note that Fig. 8(a) includes points at E_{tr} = 25, 30, 50, and 80 kcal mol^{-1} ($v = 0$, $j = 10$) calculated using only the lowest sheet of the potential energy surface, allowing us to examine the role of the conical intersection seam in the reaction Li + Li_2 → Li + Li + Li. Clearly, the results based only on one sheet nearly coincide (within the error bars) with the adiabatic cross sections for dissociation obtained using the TSH method. As the energy increases those results represent

Table 2 Summary of the trajectory calculations for the Li + $Na_2(\tilde{X}\,^1\Sigma_g^+)$ reaction[a]

			Lower sheet			Upper sheet			
E_{tr}/kcal mol^{-1}	v	b_{max}/a_0	N_{dis}^a	N_r^a	σ_d^a/a_0^2	N_{dis}^{na}	N_r^{na}	σ_d^{na}/a_0^2	$\sigma_{tot}^{(b)}/a_0^2$
17.5	0	8.70	31	432	1.5 ± 0.3	18	113	0.8 ± 0.2	2.3 ± 0.3
		6.00	34	938	0.8 ± 0.1	—	—	—	—
20.0	0	8.70	131	306	6.2 ± 0.5	160	94	7.6 ± 0.6	13.8 ± 0.8
25.0	0	8.30	192	241	8.3 ± 0.6	185	78	8.0 ± 0.6	16.3 ± 0.8
		5.50	368	625	7.0 ± 0.4	—	—	—	—
	10	11.00	285	152	21.7 ± 1.2	158	57	12.0 ± 0.9	33.7 ± 1.5
	20	13.50	479	97	54.8 ± 2.4	199	38	22.8 ± 1.6	77.6 ± 2.8
30.0	0	8.00	233	199	9.4 ± 0.6	261	77	10.5 ± 0.6	19.9 ± 0.8
35.0	0	7.70	309	135	11.5 ± 0.6	299	69	11.1 ± 0.6	22.6 ± 0.9
40.0	0	7.40	423	104	14.6 ± 0.7	368	77	12.7 ± 0.6	27.2 ± 0.9
45.0	0	7.10	566	81	17.9 ± 0.7	394	64	12.5 ± 0.6	30.4 ± 0.9
50.0	0	7.00	653	49	20.1 ± 0.7	436	57	13.4 ± 0.6	33.5 ± 0.9
		5.00	1448	167	22.7 ± 0.5	—	—	—	—
80.0	0	6.50	941	19	25.0 ± 0.7	517	50	13.7 ± 0.6	38.7 ± 0.8
		5.30	1710	38	30.2 ± 5.9	—	—	—	—

[a] For E_{tr} = 25, 50 and 80 kcal mol^{-1} (all $v = 0$), the second entry refers to the trajectory calculation where only the lower-sheet of the potential energy surface was considered. [b] Note that $\sigma_{tot} = \sigma_d^a + \sigma_d^{na}$.

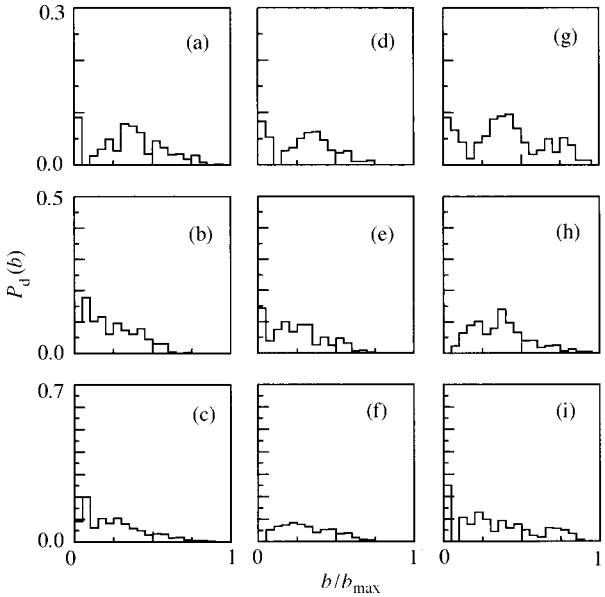

Fig. 6 As in Fig. 5 but for the nonadiabatic dissociation.

an upper bound for adiabatic dissociation, since the new open channels compete with the adiabatic ones. Thus, due to the nonadiabatic contribution for dissociation the calculations based on a single sheet always underestimate σ_{tot}.

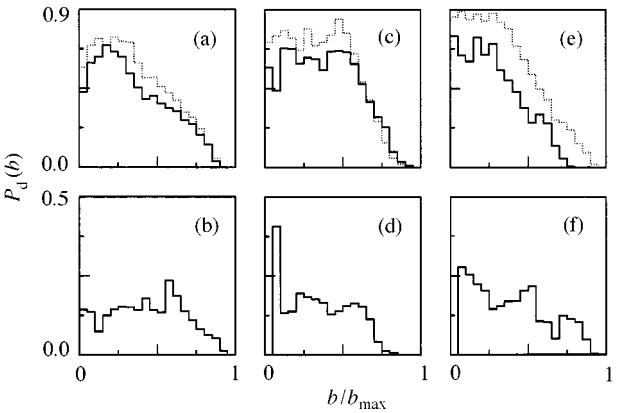

Fig. 7 Opacity function for the dissociative process at $E_{tr} = 80$ kcal mol^{-1} ($v = 0$): (a)–(b) Li + Li_2; (c)–(d) Na + Li_2; (e)–(f) Li + Na_2. Note that the panels (a), (c), and (e) refer to the adiabatic dissociation from the TSH calculations (———) or from the lowest sheet ones (·····), while panels (b), (d), and (f) show the corresponding results for the nonadiabatic dissociation.

3.2 Na + Li_2 dissociation

Table 1 summarizes the trajectory calculations for the Na + Li_2 system. The calculated dissociative cross sections are plotted in Fig. 8(b). Note that for translational energies near threshold, *i.e.*, $25 \leqslant E_{tr}$/kcal mol$^{-1} \leqslant 30$, the adiabatic and nonadiabatic dissociative cross sections coincide within the calculated error bars. For translational energies above 30 kcal mol^{-1} these two sets of results clearly diverge, the adiabatic cross sections always being larger than the nonadiabatic ones. Indeed, the latter just slightly increase for translational energies higher than 30 kcal mol^{-1} while becoming approximately constant for $E_{tr} \geqslant 50$ kcal mol^{-1}.

As a final remark on this system, we address attention to the adiabatic exchange reaction Na + $Li_2(X\,^1\Sigma_g^+, v = 0) \rightarrow$ NaLi($X\,^1\Sigma^+, v'$) + Li at $E_{tr} = 11.5$ kcal mol^{-1}. Although this is a marginal subject in the context of the present work, it is interesting to compare the result shown in Table 1 with the one obtained experimentally by Rubahn *et al.*[17] These authors estimate[17] a vanishingly small ($<3.6\ a_0^2$) reactive exchange cross section, while the value predicted from our calculation using only the lowest sheet of the potential energy surface is $\sigma_r^a = 61.3\ a_0^2$; see also ref. 18. Moreover, the hopping effects appear to have a minor role on the Na + Li_2 reaction at $E_{tr} = 11.5$ kcal mol^{-1}, since the TSH calculation of this work leads to a similar value, $\sigma_r^a = 62.9\ a_0^2$. In summary, further theoretical and experimental work is required to improve our understanding of this reactive process.

3.3 Li + Na_2 dissociation

The numerical results obtained for the Li + Na_2 system are given in Table 2, while the dissociative cross sections are shown in Fig. 8(c). Because the dissociation threshold for this system falls to 16.8 kcal mol^{-1}, we have calculated trajectories for the range of translational energies $16.5 \leqslant E_{tr}$/kcal mol$^{-1} \leqslant 80$. We may observe from Fig. 8(c) that in spite of some oscillatory behavior the adiabatic and nonadiabatic cross sections for dissociation show very similar values for translational energies up to 35 kcal mol^{-1} ($v = 0$). For higher translational energies these two sets of values diverge, leading the nonadiabatic ones to a flat curve, while the adiabatic cross sections always increase.

As for the other systems, we have performed quasiclassical trajectory calculations using only the lowest sheet of the potential energy surface for $v = 0$ at $E_{tr} = 25$, 50, and 80 kcal mol^{-1}. It is interesting to note from Table 2 the great disparity between the values of b_{max} obtained by the surface hopping trajectories and those arising from calculations in which only the lowest sheet has been used. Such a discrepancy

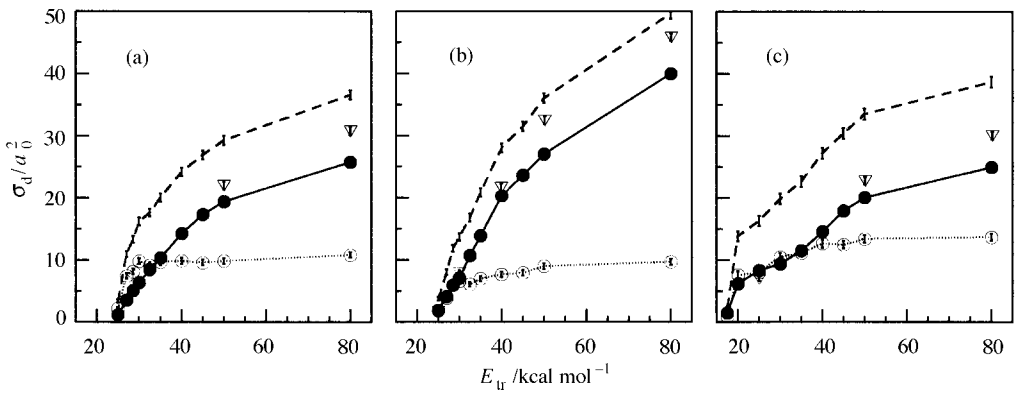

Fig. 8 Dissociative cross sections for the title reactions as a function of initial translational energy: (a) Li + Li_2; (b) Na + Li_2; (c) Li + Na_2. In the three panels the symbols and lines refer to: adiabatic dissociation (———, ●); nonadiabatic dissociation (·····, ○); total dissociation (– – – –); calculations using only the lowest sheet of the potential energy surfaces (▽).

decreases with increasing E_{tr}, suggesting a larger contribution of the nonadiabatic dissociation for impact parameters near b_{max}. This is corroborated by the opacity functions shown in Fig. 5 and 6 for $E_{tr} = 25$ kcal mol^{-1}, and Fig. 7 for $E_{tr} = 80$ kcal mol^{-1}. In fact, for the largest impact parameters, the probability of nonadiabatic dissociation becomes the most important, especially at $E_{tr} = 25$ kcal mol^{-1} for ($v = 0, j = 10$) and $E_{tr} = 80$ kcal mol^{-1}.

4 Comparison and discussion

The most noteworthy feature in Fig. 8 is the increasing behavior of all dissociative cross sections with translational energy. Although slightly different, the shape of the curves for Li + Li_2, Na + Li_2, and Li + Na_2 show a similar general pattern. As noted in Section 3, for all systems the adiabatic dissociation cross sections increase always with E_{tr}, while the nonadiabatic ones suddenly increase for energies near the threshold and then approach a nearly constant value for high translational energies. At translational energies below 35 kcal mol^{-1}, this trend leads in the case of Li + Li_2 to values for σ_d^{na} larger than σ_d^a. A slightly different behavior is obtained in that range of translational energies for Na + Li_2 and Li + Na_2 (see Tables 1 and 2). For the first system, the cross sections for adiabatic dissociation are always larger than the nonadiabatic ones, while for Li + Na_2 σ_d^a and σ_d^{na} have very similar values.

Another interesting feature from Fig. 8 for high translational energies is the fact that the total dissociative cross sections for Na + Li_2 are larger than those for Li + Li_2 (and also for Li + Na_2). Since for high energies the topographical details of the potential energy surface are expected to have a minor role on the dissociative dynamics, *i.e.*, the head-on collisions become more important to break the Li–Li bond, the larger cross sections in the case of Na + Li_2 appear to indicate that the momentum transfer is most efficient when the colliding partner is the heavier Na atom. In fact, for head-on collisions, the magnitude of the linear momentum can be represented for a given translational energy E_{tr} by

$$p = (2E_{tr}\mu)^{1/2} \quad (3)$$

Since the reduced masses μ for the three systems follow the order $\mu_{Na+Li_2} > \mu_{Li+Na_2} > \mu_{Li+Li_2}$, the total dissociative cross sections also follow that order at the highest translational energies, in agreement with eqn. (3). Note that, for translational energies just above threshold, the dissociative process is not the dominant one, and the topographical differences between the potential energy surfaces for the three systems should play a fundamental role in deciding whether a trajectory leads to dissociation or to any other outcome. Due to this, we obtain larger values for the total dissociative cross sections for Li + Li_2 at the referred low energy range. Note also that, for Li + Na_2, the threshold arises at lower energies than for Li + Li_2 and Na + Li_2, which requires a shift of the corresponding curves to the right-hand-side in order to allow a proper comparison. Thus, it is not unexpected that one obtains significantly larger values for the dissociative cross sections in Li + Na_2 than for the two other systems at 25 kcal mol^{-1}.

Fig. 8 shows also the dissociative cross sections obtained using only the lowest sheet of the respective potential energy surface, while Fig. 9 presents the probabilities both for dissociation and reactive exchange of atoms. It is clear from these figures that, for high energies where dissociation is the dominant process, the calculations using only the lowest sheet of the potential energy surfaces give dissociative cross sections above the values of σ_d^a obtained from the TSH calculations. This is particularly relevant for $E_{tr} = 50$ and 80 kcal mol^{-1}, and has been rationalized[1] by recognizing that the conical intersection opens a new route for reaction. Because of this possibility of hopping from one sheet to another, the dynamics becomes more intricate especially for energies at which the trajectory has the chance to go up and down, *e.g.* $E_{tr} = 25$ kcal mol^{-1}. Hence, for these translational energies, all the adiabatic channels are influenced by the dynamics associated with the conical intersection which prevents an easy comparison between the TSH calculations and the results obtained using only the lowest sheet of the potential energy surfaces. Indeed, for $E_{tr} = 25$ kcal mol^{-1}, the dissociative cross sections obtained from the lowest sheet calculations underestimate the corresponding TSH results, σ_d^a, especially for the Li + Na_2 system. Conversely, the adiabatic exchange probabilities are always above the corresponding values obtained from the TSH method.

A very interesting feature in Fig. 8 is the similar behavior of the nonadiabatic dissociative cross sections for all the title systems. The general pattern of the corresponding curves can be described by a fast initial increase followed by a constant or slightly rising behavior of the cross section. This can be related to two distinct energy regimes: (a) the close to threshold regime which goes up to 30 kcal mol^{-1} for Li + Li_2 while extending a little bit further for Na + Li_2 and Li + Na_2, where there is a clear competition between the different channels; (b) the high energy regime (flat region). We begin by rationalizing regime (a). In this case, the sudden increase of σ_d^{na}

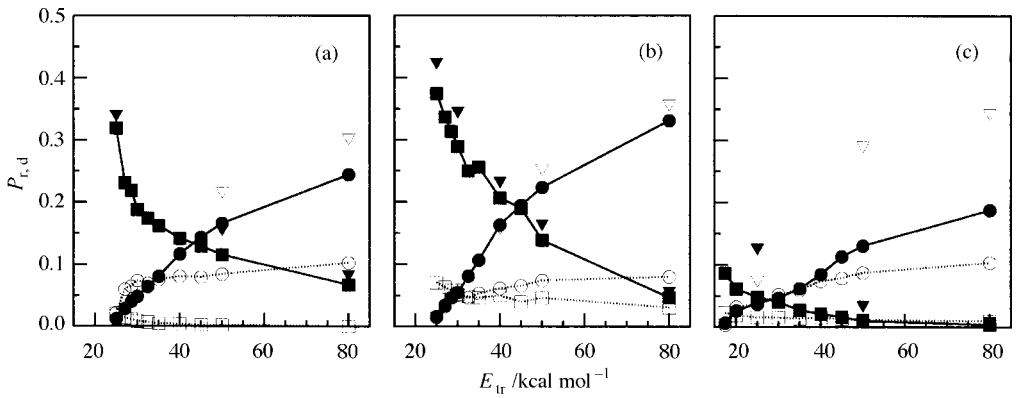

Fig. 9 Reactive and dissociative probabilities as a function of initial translational energy: (a) Li + Li_2; (b) Na + Li_2; (c) Li + Na_2. Calculations involving the two sheets of potential energy surfaces: ———, processes occurring *via* the lower sheet; ·····, processes occurring *via* the upper sheet; ●, adiabatic dissociation; ■, exchange reaction; ○, nonadiabatic dissociation; □, all three reactive events occurring *via* the upper sheet. Calculations involving only the lowest sheet at $E_{tr} = 25$, 50, and 80 kcal mol^{-1} [panel (a)], $E_{tr} = 25$, 30, 40, 50, and 80 kcal mol^{-1} [panel (b)], and $E_{tr} = 17.5$, 25, 50, and 80 kcal mol^{-1} [panel (c)]: ▽, dissociation; ▼, exchange reaction.

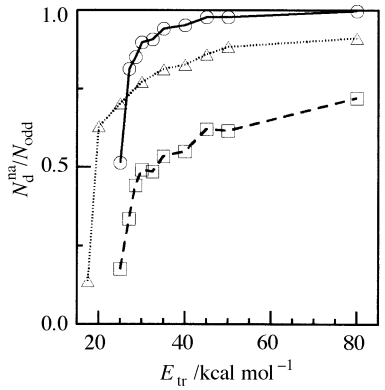

Fig. 10 Efficiency for dissociation *via* the upper sheet: Li + Li_2 (○, ———); Na + Li_2 (□, – – – –); Li + Na_2 (△, ·····).

is mainly due to the fast decrease of the adiabatic exchange probability, as clearly seen from Fig. 9. Obviously, this trend in the exchange probability contributes also to the increase of the adiabatic dissociation cross sections shown in Fig. 8.

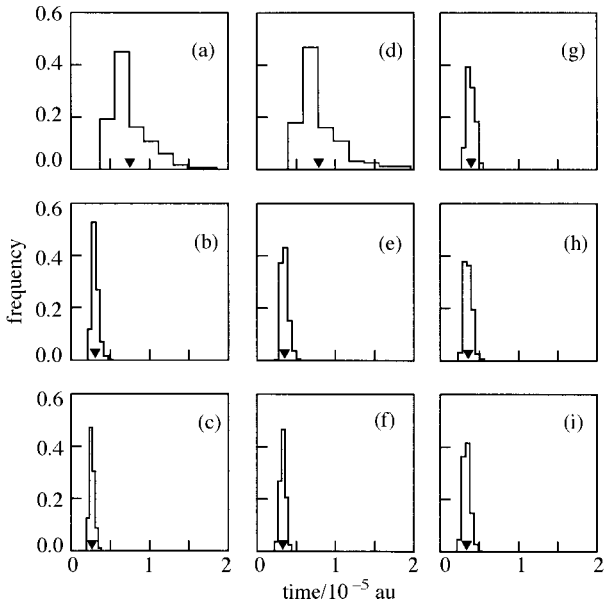

Fig. 11 Dissociative trajectory lifetime distribution: (a)–(c) Li + Li_2 ; (d)–(f) Na + Li_2 ; (g)–(i) Li + Na_2. The initial translational energy was fixed at $E_{tr} = 25$ kcal mol^{-1}, while the vibrational quantum number has taken the values $v = 0$ [(a), (d), and (g)], $v = 10$ [(b), (e), and (h)], and $v = 20$ [(c), (f), and (i)]. The arrows indicate the mean values of the trajectory lifetime. For Li + Li_2 they are 0.75×10^5 au ($v = 0$), 0.30×10^5 au ($v = 10$), and 0.26×10^5 au ($v = 20$); for Na + Li_2 they are 0.79×10^5 au ($v = 0$), 0.35×10^5 au ($v = 10$), and 0.33×10^5 au ($v = 20$); for Li + Na_2 they are 0.40×10^5 au ($v = 0$), 0.36×10^5 au ($v = 10$), and 0.34×10^5 au ($v = 20$).

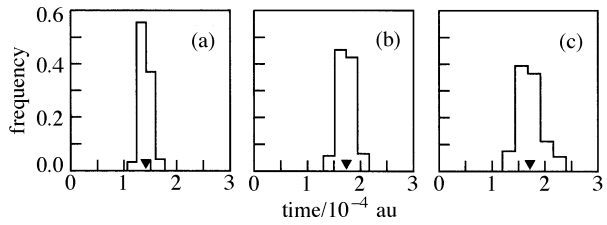

Fig. 12 As in Fig. 11, but for the initial translational energy fixed at $E_{tr} = 80$ kcal mol^{-1} and $v = 0$: (a) Li + Li_2 ; (b) Na + Li_2 ; (c) Li + Na_2. The arrows indicate the mean values of the trajectory lifetime, *i.e.*, 1.4×10^4 au for Li + Li_2, 1.7×10^4 au for Na + Li_2, 1.7×10^4 au for Li + Na_2.

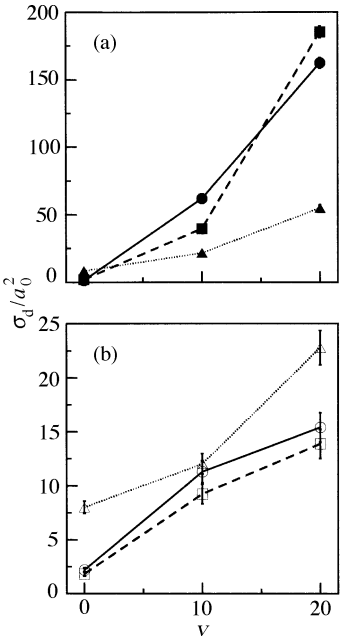

Fig. 13 Dissociative cross sections for $E_{tr} = 25$ kcal mol^{-1} as a function of the initial vibrational quantum number v: (a) adiabatic dissociation; (b) nonadiabatic dissociation. In both panels, the symbols and lines refer to: Li + Li_2 (———, ●, ○); Na + Li_2 (– – – –, □, ■); Li + Na_2 (·····, △, ▲).

Additionally, the nonadiabatic dissociation competes with the other upper sheet reactive channels as displayed in Fig. 10. Note that the nonadiabatic efficiency curves presented in Fig. 10 for the title systems resemble the corresponding behavior of σ_d^{na}. Note especially that the efficiency curves show a sudden increase at regime (a), approaching quickly the maximum value in the case of Li + Li_2 which contributes to having higher values of σ_d^{na} than σ_d^a. In contrast, one observes a worse performance in the case of Na + Li_2, while Li + Na_2 provides an intermediate situation. The difference in efficiency for the three systems is well understood by the observation of the energetics diagram in Fig. 4. It is seen that a smaller amount of energy is required to break the electronically excited $Li_2(b\,^3\Sigma_u^+)$ molecule than the corresponding diatomics in the cases of Li + Na_2 [*i.e.*, $Na_2(b\,^3\Sigma_u^+)$ and LiNa ($^3\Sigma^+$)] and Na + Li_2 [*i.e.*, $Li_2(b\,^1\Sigma_u^+)$ and LiNa($^3\Sigma^+$)].

As the translational energy increases, the efficiency no longer contributes significantly to nonadiabatic dissociation (*i.e.*, the efficiency curves become flatter), especially for Li + Li_2 and Li + Na_2, and the corresponding cross sections tend to follow the (b)-type behavior. In fact, the adiabatic dissociation always depends only on the bond-breaking energetic aspects while for the nonadiabatic dissociation these features must be considered together with the chance of hopping, since the dissociative trajectories must occur *via* upper sheet. Thus, the energetic features are most important near threshold, while the chance of hopping becomes crucial at high energies. In turn, the chance of hopping depends on the Landau–Zener probability for electronic transition, which increases with velocity (*i.e.*, with E_{tr}), and the number of times that the trajectory crosses the crossing seam. Of course, the latter is dominated by the particular definition of the seam, the topographical aspects of the potential energy surface (mainly close to the conical intersection), and the amount of time that the trajectory lasts. Since the first and second issues are predefined for the three systems, we look only at the variation of the trajectory lifetimes as a function of the initial translational energy. They are shown in Fig. 11 and Fig. 12 for the dissociative processes at $E_{tr} = 25$ and 80 kcal mol^{-1}, respectively. As expected, the trajectory lifetimes decrease with increasing

translational energy, which coincides with a reduction in the number of seam crosses computed for the title systems at those extreme values of E_{tr}. Indeed, for $Li + Li_2$ the mean value of the number of crosses per dissociative trajectory decreases from 8.0 at $E_{tr} = 25$ kcal mol^{-1} to 2.6 at $E_{tr} = 80$ kcal mol^{-1}, while for $Na + Li_2$ and $Li + Na_2$ the corresponding values are 7.8 and 2.6, and 3.8 and 2.9, respectively. This implies that the opportunity of hopping decreases with increasing translational energy, since in the present method the trajectory is only allowed to hop when it passes the crossing seam. Thus, the opposing trends of the Landau–Zener probability and number of seam crosses per trajectory with increasing translational energy may explain the flat behavior encountered for the nonadiabatic dissociative cross sections.

We now discuss the influence of the initial vibrational energy in the dissociation process. Fig. 13 presents the dependence of the dissociative cross section for the $Li + Li_2$, $Na + Li_2$ and $Li + Na_2$ systems on the initial vibrational quantum number v of Li_2 or Na_2 molecules. The corresponding numerical values for $Li + Li_2$ have been given elsewhere[1] while, for the systems $Na + Li_2$ and $Li + Na_2$, they are presented in Tables 1 and 2, respectively. As follows from Fig. 13, the dissociative cross sections (adiabatic and nonadiabatic) follow similar trends for both $Li + Li_2$ and $Na + Li_2$. This is not a surprising result since we are in both cases breaking a similar Li–Li bond (see Fig. 4), being the differences due to the distinct approaching atom, *i.e.*, Li or Na. Moreover, the adiabatic cross sections of Fig. 13(a) show a fast increase with v, especially for the $Li + Li_2$ and $Na + Li_2$ systems, which is due to the increase of the maximum impact parameter and probability of dissociation. In contrast, the nonadiabatic cross sections shown in Fig. 13(b) are seen to just slightly increase with the vibrational quantum number. These trends can be rationalized by examining the distribution of trajectories according to the number of hops in the lower and upper sheets of the corresponding potential energy surfaces. They are presented in Table 3 for $E_{tr} = 25.0$ kcal mol^{-1} and $v = 0$, 10, 20. Table 3 shows a drastic increase in the number of trajectories with zero hops on going from $v = 0$ to $v = 20$, and a slow dependence on v for the odd number of hops which lead to nonadiabatic dissociation. In fact, the number of hops per dissociative trajectory decreases with increasing v, which again coincides with a corresponding decrease in the trajectory lifetime as displayed in Fig. 11 for all title systems. Furthermore, Fig. 13 shows that the adiabatic dissociative cross section for $Li + Na_2$ is clearly below that calculated for $Li + Li_2$ and $Na + Li_2$ as v increases to 10 and 20, while the corresponding nonadiabatic values appear in the reverse order. Concerning the adiabatic cross sections, the observed trends may be rationalized from the larger internal states spacing in Li_2 than in Na_2, which implies a larger increase in the available energy to promote dissociation as v increases to 10 and 20; see Fig. 4. However, as it has been pointed out above, the nonadiabatic dissociation depends also on the chance of hopping which should become larger for $Li + Na_2$ (since we obtain longer trajectory lifetimes for this system; see Fig. 11) as v increases to 10 and 20. Indeed, as explained before for the dependence of σ_d^{na} on E_{tr}, we expect the chance of hopping to be crucial at the highest energies, *i.e.*, for $v = 10$ and 20.

5 Conclusion

The present study of collision-induced dissociation of $Li + Li_2$, $Na + Li_2$ and $Li + Na_2$ systems on realistic two-valued potential energy surfaces has shown that the conical intersection plays a significant role in the dynamics of the dissociation and exchange reactions. In particular, we have observed an increase of the nonadiabatic cross sections for translational energies close to threshold, becoming for all title systems approximately constant at high values of E_{tr}. Since the TSH method used in this work only allows the electronic transition when the trajectory crosses the intersection seam, the dependence of nonadiabatic cross sections on energy is dominated by the number of such crosses, especially for the higher range of translational energies. It has also been stressed that this essentially depends on two factors: (a) topography of potential energy surfaces, and (b) trajectory lifetime. Clearly, the first dominates at low energies while the second becomes crucial as the translational energy increases. In this context, we have noted that the increase in the internal energy of the reactant diatomic does not contribute to increasing the number of hops per dissociative trajectory which leads to a weak dependence of nonadiabatic dissociation on v for all title systems. Furthermore, it has been shown that the different mass relations for the three title systems leads to larger values of the adiabatic cross sections in the case of $Na + Li_2$ at high energies. This has been attributed to the efficiency of linear momentum transfer for head-on collisions at high energies. Moreover, the dependence of adiabatic cross sections on the vibrational quantum number essentially depends on the available energy content, which is largest for $Li + Li_2$ and $Na + Li_2$, and on the efficiency of linear momentum transfer for head-on collisions, which may be responsible for the cross-

Table 3 Distribution of trajectories according to the number of hops occurring during the $Na + Li_2$ ($Li + Na_2$) dissociative processes in the lower sheet (with even number of hops) and the upper sheet (with odd number of hops) for each set of initial conditions

E_{tr}/ kcal mol^{-1}	v	Even number of hops						Odd number of hops			
		N_0	N_2	N_4	N_6	N_8	N_{10}	N_1	N_3	N_5	N_7
17.5	0	(18)	(8)	(4)	(1)	(0)	(0)	(12)	(4)	(2)	(0)
20.0	0	(55)	(12)	(53)	(11)	(0)	(0)	(102)	(48)	(9)	(7)
25.0	0	60(103)	11(29)	6(54)	2(5)	1(1)	0(0)	59(113)	14(67)	1(5)	2(0)
	10	421(186)	14(39)	4(54)	0(6)	0(0)	0(0)	83(70)	18(78)	1(9)	0(1)
	20[a]	1365(333)	38(104)	0(34)	1(8)	0(0)	0(0)	80(54)	22(136)	2(8)	1(0)
27.0	0	138	18	10	1	0	1	127	31	1	0
28.5	0	202	21	6	2	0	0	202	28	1	0
30.0	0	238(149)	31(41)	4(32)	0(10)	0	0(1)	219(152)	29(97)	3(12)	0(0)
32.5	0	353	48	3	0	0	0	199	29	1	0
35.0	0	467(192)	61(57)	2(49)	2(11)	0(0)	0(0)	239(183)	27(101)	1(13)	0(2)
40.0	0	730(290)	84(69)	1(55)	1(8)	0(1)	0(0)	269(218)	39(134)	0(16)	0(0)
45.0	0	876(399)	100(95)	0(60)	1(12)	0(0)	0(0)	290(206)	38(173)	0(15)	0(0)
50.0	0	998(490)	121(100)	2(55)	0(8)	0(0)	0(0)	333(245)	39(173)	0(16)	0(2)
80.0	0	1516(757)	140(117)	1(58)	0(9)	0(0)	0(0)	358(287)	43(215)	0(13)	0(2)

[a] Although not represented in this table, for $v = 20$ we obtain one $Li + Na_2$ dissociative trajectory with 11 hops.

ing of the $Li + Li_2$ and $Na + Li_2$ curves when going from $v = 10$ to $v = 20$.

Acknowledgements

The financial support from Fundação para a Ciência e Tecnologia, Portugal, under programmes PRAXIS XXI and FEDER is gratefully acknowledged.

References

1 A. I. Voronin, J. M. C. Marques and A. J. C. Varandas, *J. Phys. Chem. A*, 1998, **102**, 6057.
2 A. J. C. Varandas and A. A. C. C. Pais, *J. Chem. Soc., Faraday Trans.*, 1993, **89**, 1511.
3 A. A. C. C. Pais, R. F. Nalewajski and A. J. C. Varandas, *J. Chem. Soc., Faraday Trans.*, 1994, **90**, 1381.
4 A. J. C. Varandas, *Adv. Chem. Phys.*, 1988, **74**, 255.
5 A. J. C. Varandas, *Chem. Phys. Lett.*, 1992, **194**, 333.
6 A. J. C. Varandas and R. F. Nalewajski, *Chem. Phys. Lett.*, 1993, **205**, 253.
7 V. M. F. Morais and A. J. C. Varandas, *Mol. Phys.*, 1995, **84**, 957.
8 A. A. C. C. Pais, A. I. Voronin and A. J. C. Varandas, *J. Phys. Chem.*, 1996, **100**, 7480.
9 A. J. C. Varandas, V. M. F. Morais and A. A. C. C. Pais, *Mol. Phys.*, 1986, **58**, 285.
10 A. J. C. Varandas and V. M. F. Morais, *Mol. Phys.*, 1982, **47**, 1241.
11 A. J. C. Varandas and J. Brandão, *Mol. Phys.*, 1982, **45**, 857.
12 J. C. Tully and R. K. Preston, *J. Chem. Phys.*, 1971, **55**, 562.
13 N. C. Blais, D. G. Truhlar and C. A. Mead, *J. Chem. Phys.*, 1988, **89**, 6204.
14 J. C. Tully, *J. Chem. Phys.*, 1990, **93**, 1061.
15 M. S. Topaler, M. D. Hack, T. C. Allison, Y.-P. Liu, S. L. Mielke, D. W. Schwenke and D. G. Truhlar, *J. Chem. Phys.*, 1997, **106**, 8699.
16 M. S. Topaler, T. C. Allison, D. W. Schwenke and D. G. Truhlar, *J. Phys. Chem. A*, 1998, **102**, 1666.
17 H.-G. Rubahn, A. Slenczka and J. P. Toennies, *J. Chem. Phys.*, 1994, **101**, 1262.
18 H.-G. Rubahn and N. Sathyamurthy, *Mol. Phys.*, 1993, **78**, 1047.

Paper 9/01669D